

2017

# Robotic 3D Plant Perception and Leaf Probing with Collision-Free Motion Planning for Automated Indoor Plant Phenotyping

Yin Bao

*Iowa State University*, [yinbao@iastate.edu](mailto:yinbao@iastate.edu)

Lie Tang

*Iowa State University*, [lietang@iastate.edu](mailto:lietang@iastate.edu)

Dylan Shah

*Iowa State University*

Follow this and additional works at: [https://lib.dr.iastate.edu/abe\\_eng\\_conf](https://lib.dr.iastate.edu/abe_eng_conf)



Part of the [Agriculture Commons](#), and the [Bioresource and Agricultural Engineering Commons](#)

The complete bibliographic information for this item can be found at [https://lib.dr.iastate.edu/abe\\_eng\\_conf/566](https://lib.dr.iastate.edu/abe_eng_conf/566). For information on how to cite this item, please visit <http://lib.dr.iastate.edu/howtocite.html>.

---

This Conference Proceeding is brought to you for free and open access by the Agricultural and Biosystems Engineering at Iowa State University Digital Repository. It has been accepted for inclusion in Agricultural and Biosystems Engineering Conference Proceedings and Presentations by an authorized administrator of Iowa State University Digital Repository. For more information, please contact [digirep@iastate.edu](mailto:digirep@iastate.edu).

---

# Robotic 3D Plant Perception and Leaf Probing with Collision-Free Motion Planning for Automated Indoor Plant Phenotyping

## **Abstract**

Various instrumentation devices for plant physiology study such as chlorophyll fluorimeter and Raman spectrometer require leaf probing with accurate probe positioning and orientation with respect to leaf surface. In this work, we aimed to automate this process with a Kinect V2 sensor, a high-precision 2D laser profilometer, and a 6-axis robotic manipulator in a high-throughput manner. The relatively wide field of view and high resolution of Kinect V2 allowed rapid capture of the full 3D environment in front of the robot. Given the number of plants, the location and size of each plant were estimated by K-means clustering. A real-time collision-free motion planning framework based on Probabilistic Roadmap was adopted to maneuver the robotic manipulator without colliding with the plants. Each plant was scanned from top with the short-range profilometer to obtain a high-precision point cloud where potential leaf clusters were extracted by region growing segmentation. Each leaf segment was further partitioned into small patches by Voxel Cloud Connectivity Segmentation. Only the small patches with low root mean square values of plane fitting were used to compute probing poses. To evaluate probing accuracy, a square surface was scanned at various angles and its centroid was probed perpendicularly with a probing position error of 1.5 mm and a probing angle error of 0.84 degrees on average. Our growth chamber leaf probing experiment showed that the average motion planning time was 0.4 seconds and the average traveled distance of tool center point was 1 meter.

## **Keywords**

3D perception, high-throughput, motion planning, plant phenotyping, robotic leaf probing

## **Disciplines**

Agriculture | Bioresource and Agricultural Engineering

## **Comments**

This proceeding is published as Bao, Yin, Lie Tang, and Dylan Shah. "Robotic 3D Plant Perception and Leaf Probing with Collision-Free Motion Planning for Automated Indoor Plant Phenotyping." ASABE Annual International Meeting, Spokane, WA, July 16-19, 2017. Paper No.1700369. DOI: [10.13031/aim.201700369](https://doi.org/10.13031/aim.201700369). Posted with permission.



2950 Niles Road, St. Joseph, MI 49085-9659, USA  
269.429.0300 fax 269.429.3852 hq@asabe.org www.asabe.org

*An ASABE Meeting Presentation*

*DOI: 10.13031/aim.201700369*

*Paper Number: 1700369*

## ***Robotic 3D Plant Perception and Leaf Probing with Collision-Free Motion Planning for Automated Indoor Plant Phenotyping***

***Yin Bao, Lie Tang, Dylan Shah***

***Iowa State University***

**Written for presentation at the  
2017 ASABE Annual International Meeting**

**Sponsored by ASABE**

**Spokane, Washington**

**July 16-19, 2017**

**ABSTRACT.** *Various instrumentation devices for plant physiology study such as chlorophyll fluorimeter and Raman spectrometer require leaf probing with accurate probe positioning and orientation with respect to leaf surface. In this work, we aimed to automate this process with a Kinect V2 sensor, a high-precision 2D laser profilometer, and a 6-axis robotic manipulator in a high-throughput manner. The relatively wide field of view and high resolution of Kinect V2 allowed rapid capture of the full 3D environment in front of the robot. Given the number of plants, the location and size of each plant were estimated by K-means clustering. A real-time collision-free motion planning framework based on Probabilistic Roadmap was adopted to maneuver the robotic manipulator without colliding with the plants. Each plant was scanned from top with the short-range profilometer to obtain a high-precision point cloud where potential leaf clusters were extracted by region growing segmentation. Each leaf segment was further partitioned into small patches by Voxel Cloud Connectivity Segmentation. Only the small patches with low root mean square values of plane fitting were used to compute probing poses. To evaluate probing accuracy, a square surface was scanned at various angles and its centroid was probed perpendicularly with a probing position error of 1.5 mm and a probing angle error of 0.84 degrees on average. Our growth chamber leaf probing experiment showed that the average motion planning time was 0.4 seconds and the average traveled distance of tool center point was 1 meter.*

**Keywords.** *3D perception, high-throughput, motion planning, plant phenotyping, robotic leaf probing.*

### **1. Introduction**

Agricultural robotics is undergoing a rapid growth propelled by the need of automated high-throughput plant phenotyping

The authors are solely responsible for the content of this meeting presentation. The presentation does not necessarily reflect the official position of the American Society of Agricultural and Biological Engineers (ASABE), and its printing and distribution does not constitute an endorsement of views which may be expressed. Meeting presentations are not subject to the formal peer review process by ASABE editorial committees; therefore, they are not to be presented as refereed publications. Publish your paper in our journal after successfully completing the peer review process. See [www.asabe.org/JournalSubmission](http://www.asabe.org/JournalSubmission) for details. Citation of this work should state that it is from an ASABE meeting paper. EXAMPLE: Author's Last Name, Initials. 2017. Title of presentation. ASABE Paper No. ---. St. Joseph, MI.: ASABE. For information about securing permission to reprint or reproduce a meeting presentation, please contact ASABE at [www.asabe.org/permissions](http://www.asabe.org/permissions) (2950 Niles Road, St. Joseph, MI 49085-9659 USA).

in recent years. Many phenotyping robots to date focus on imaging plants with various cameras (RGB, hyperspectral, thermal, etc.) and 3D reconstruction with different range sensors (stereo, Time-of-Flight, LiDAR, etc.). Few systems address automatic instrumentation of molecular activity and composition for plant physiology study. Chlorophyll fluorometer is widely used to measure chlorophyll fluorescence which is an indication of photosynthesis and plant stress type. Raman spectrometer can be used to identify and quantify valuable plant substances (Schulz, Baranska, 2007). These devices require positioning a fiber optic probe on top of plant leaf at a close distance and a certain angle. For example, MINI-PAM-II from WALZ (Effeltrich, Germany) measures fluorescence with a fiberoptics as the probe. The standard leaf clip has a 60-degree angle between sample plane and fiberoptics. The distance between them is adjustable but normally 8 mm. Agility Raman Spectrometer from BaySpec (California, USA) also uses a fiber-optic probe. The probing angle is 90 degree and the probing distance depends on the focus distance of lens in the probe where typical values are 6mm and 15 mm. Automated leaf probing for above instruments is highly challenging in two aspects. First, it needs to solve 3D detection of individual plant leaf in a complex scene with partially occluded leaves. Different species may have different leaf shapes. Even within the same species, plant leaves grow and may curl at some point. Second, a robotic manipulator with at least 5 degrees of freedom (DOF) is necessary to position the probe with respect to the leaf surface. To bring the probe in position, motion planning of each robot joint should be carried out to avoid collision with the plants.

Robotic leaf probing research has mostly focused on leaf segmentation. Alenyà et al. (2013) developed an eye-in-hand system with a multi-axis robot arm and a ToF range sensor to grip a leaf from the side with a customized disk-cutting tool. A depth segmentation algorithm was developed to extract the single leaf segment in front of the ToF sensor using both the intensity and depth images. A grasping point was predetermined on a leaf contour model. By fitting the model to the segmented leaf the grasping point was found and probing was performed. In the following work, Foix et al. (2015) developed an active exploration process to incrementally gain more information about the leaf in view until the probing could be performed. A depth sensor was fixed to acquire the top-view the whole plant and to facilitate motion planning. Ahlin et al. (2016) used deep convolutional neural network to detect plant leaves in the images acquired by a RGB camera mounted on the end-effector. Sparse feature points between frames were used to compute 3D location of the leaves for guiding the end-effector. But this work only addressed bringing the end-effector close to the leaf.

Previous related work focused on probing a single plant in front of the robot. The Enviratron project at Iowa State University aims at a fully automated facility to monitor performance of plants under different environmental conditions in eight customized growth chambers. Our ultimate goal is to develop a mobile robot that can carry different types of sensors and probes and enter the vestibule on the back of each growth chamber to collect sensor data for multiple plants. The key tasks for the robot inside the vestibule are to localize each plant, detect individual leaf and probe the appropriate leaves without damaging the plants or the growth chamber. In this work, we propose a robotic leaf probing pipeline using an eye-in-hand robotic system including a Kinect V2 sensor, a high-precision 2D laser profilometer and a 6-DOF robotic manipulator. The Time-of-Flight (ToF) camera of Kinect V2 outputs depth images with a resolution of 512×424 and a field of view (FOV) of 70×60 degrees. Such wide FOV and high resolution make it a suitable sensor for rapid mapping of the 3D environment in front of the robot. The 3D point cloud is used to localize each plant and estimate its size. In addition, the same point cloud defines the occupied workspace which the robotic manipulator should avoid. Despite low cost and the efficiency in environment mapping, the depth sensing of Kinect V2 tends to be noisy due to the nature of ToF. However, robotic leaf probing relies on accurate surface normal estimation to compute the required angle between leaf surface patch and probe. Therefore, a short-range high-precision 2D laser profilometer is used to scan individual plant from top with a sweeping motion of the end-effector. Thanks to the high precision, accurate surface normal and curvature can also be utilized in region growing segmentation for piece-wise smooth plant leaves. Furthermore, a leaf segment is partitioned into point clusters of similar sizes and the probing poses (position and orientation) of the end-effector are computed for the clusters with low root mean square (RMS) values of plane fitting. To move the probe from a starting pose to the probing pose, motion planning in 6-dimension configuration space (C-space/joint space) searches for a sequence of collision-free configurations where the swept volume between any two consecutive configurations only occupies free 3D space. Such motion planning in high dimensional space is computationally expensive due to the expensive evaluation of volume/swept-volume in 3D space given one/two configuration(s) in C-space. Minimum robot operation time means minimum disturbance to plant growth. Therefore, we adopted a real-time motion planning framework which pre-builds a reusable data structure that links cells in 3D grid to random configurations in C-space and requires minimum computation during online planning.

Our specific objectives of this study were:

1. To develop a robotic leaf probing system with 3D plant perception and collision-free motion planning capabilities for a growth chamber environment.
2. To quantify the system accuracy in terms of probing position and probing angle.
3. To evaluate the motion planning performance for leaf probing in a growth chamber environment.

## 2. Materials and Methods

### 2.1. Robot

Our robot consists of three modules, an unmanned ground vehicle (UGV), a 6-axis robotic manipulator, and a sensing unit (Shah et al., 2016). The UGV is custom-built with omnidirectional Mecanum wheels and magnetic guide sensors. The robotic manipulator is a Universal Robots UR10 (Odense, Denmark) with a reach radius of 1.3 m and a repeatability of  $\pm 0.1$  mm. The sensing unit includes a Kinect V2 sensor (Washington, USA) and a Keyence LJ-V7300 2D in-line laser profilometer (Osaka, Japan). The distance measurement of Kinect V2 could deviate from the true distance up to approximately 0.03m within a range of 0.4 m to 6 m (Lachat et al., 2015). Despite its relatively low accuracy in depth sensing, Kinect was successfully used for real-time 3D modelling of natural scenes (Newcombe et al., 2011). Its long sensing range and wide FOV makes it suitable for 3D mapping of a growth chamber environment since the plant location and size are considered unknown. On the other hand, the laser profilometer has a relatively short measurement range of 0.155 m to 0.445 m but a high depth repeatability of 0.005 mm. This type of sensor is often used for surface profile inspection in manufacturing industry. With the accurate motion control of a modern industrial robotic manipulator, high-precision 3D scan is easily obtained and necessary for accurate probe positioning and reliable local surface normal estimation. Therefore, the two sensors serve unique purposes in our system.

### 2.2. Real-Time Collision-Free Motion Planning

Motion planning plays a critical role for robotic leaf probing. Not all plant leaves are possible for the robotic manipulator to probe given the complex environment in a growth chamber. There could be no collision-free inverse kinematic solution for the probing pose or no path to reach the probing pose without colliding the environment. Motion planning for high-dimensional configuration space has been well studied during the last three decades. The current state-of-the-art are built upon sampling-based algorithms such as Probabilistic Roadmap (Kavraki et al., 1996) and Rapidly-Exploring Random Tree (LaValle, 1998). The basic idea is to explore the configuration space by random sampling and connect neighboring configurations if the paths are collision-free in 3D workspace. A shortest path between a start configuration and a goal configuration on this network is searched by some graph search algorithm. Leven and Hutchinson (2002) proposed a real-time motion planning framework for changing environments based on Probabilistic Roadmap (PRMCE). First it builds the roadmap assuming that there is no obstacle in workspace. Next it discretizes the workspace surrounding the robotic manipulator with a 3D occupancy grid. In addition to the occupancy status, each cell in the grid stores a list of all the nodes (configurations) in the roadmap in collision with the cell. When a cell becomes occupied, the associated nodes are temporarily blocked until the cell is free. In this way, any path on the roadmap is always collision-free. The roadmap and occupancy grid only have to be computed once although it may take a long time due to collision checking for the nodes and the edges. Motion planning mainly requires a graph search and takes minimum time. The framework was tested in a simulated environment. Kunz et al. (2010) improved PRMCE for a real 7-DOF robotic manipulator and used a fixed depth camera to update the 3D occupancy grid in real time. Less than 100 ms was reported for obstacle detection and path planning. Recently, Murray et al. (2016) implemented PRMCE on a field-programmable gate array (FPGA) and achieved real-time motion planning on a chip. All the advances proved the practical value of PRMCE. Therefore, we customized PRMCE for our robotic leaf probing system.

#### 2.2.1. Robot Modeling and Self-Collision Checking

To efficiently perform collision checking, we model the robot components (probe, sensors, robot arms, and mobile base) using oriented bounding box (OBB). During creation of roadmap, random generation of joint positions may result in self-collision. Based on the separating axis theorem, collision checking of two OBBs comes down to at most 15 non-intersection tests (Eberly, 2002). If any two robot components which can be moved relatively (e.g. first arm and second arm) do not collide, the configuration is free of self-collision. Since our robot stops at a fixed location with respect to the growth chamber, we incorporated some parts of the growth chamber into the robot model such that self-collision checking also checks collision with growth chamber. Figure 1 visualizes the robot modeling with OBBs.

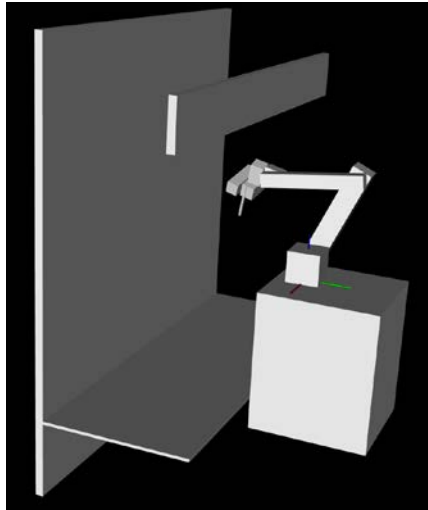


Figure 1. Robot and partial growth chamber modeling with oriented bounding boxes.

### 2.2.2. Roadmap Generation

To create the roadmap,  $N$  random self-collision-free configurations need to be generated as vertices in a weighted graph. The six joint positions are randomly sampled from a uniform distribution. Since our robotic manipulator normally moves inside the growth chamber, each joint is limited to a specific range with the maximum range less than 180 degrees. A range of 45 degrees is allowed for the last joint (end-effector) to prevent twisting the sensor cables. To create edges in the graph, we connect each vertex to its  $K$ -nearest neighbors. The weight of an edge equals the distance between the two connected configurations measured as the Euclidian norm of  $M$  reference points on the robotic manipulator. The reference points are the origins of the reference frames defined by the Denavit-Hartenberg parameters (Figure 2). Therefore, the distance metric measures the overall displacement of all joints in 3D workspace. As the joint range never exceeds 180 degrees, we avoid the use of more complicated distance metric (Kunz et al., 2010) in case that the Euclidian norm of a reference point can be short whereas the swept-volume of an arm is large as demonstrated in Figure 3.

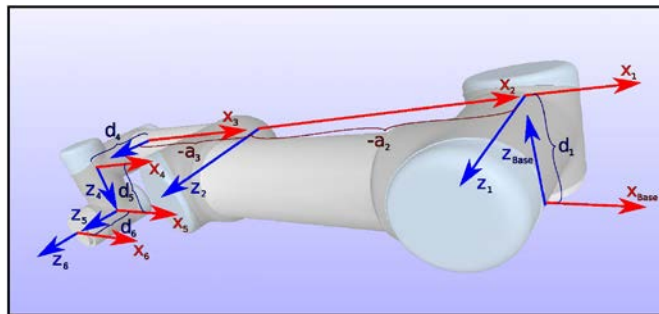


Figure 2. Reference frames defined by the Denavit-Hartenberg parameters for UR10 (Universal Robots Support).

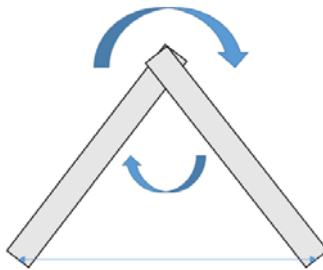


Figure 3. Ambiguity of using the Euclidian norm of a reference point in 3D space as the distance metric when joint rotation angle is allowed to exceed 180 degrees.

### 2.2.3. Mapping Workspace to Roadmap

Swept volume is represented as a set of cells in the 3D occupancy grid. The volume of a single configuration can be computed by voxelizing the OBBs of the robotic manipulator and sensors in the 3D grid. Our OBB voxelization is based on 3D line voxelization (Cohen-Or & Kaufman, 1997). We first voxelize two parallel edges of a rectangle face on the OBB and then use the two edges to rasterize the face. Finally, we extrude the face to the size of the OBB and obtain the set of cells in the volume. To compute the swept volume, we start with the volume of the two end configurations and then compute volume of the halfway configuration. We continue the recursive voxelization until there is no new cell found.

An edge in the roadmap corresponds to the swept volume between two configurations. For mapping workspace to roadmap, every cell in the 3D occupancy grid needs to maintain a list of edges whose associated volume contains the cell. We visit each edge and voxelize the swept volume and then add the edge to all the cells traversed by voxelization.

#### 2.2.4. Online Planning

During online stage, the point cloud data from both Kinect V2 and 2D laser profilometer are used to update the 3D occupancy grid. If a cell is occupied, we make the weights of the associated edges temporally infinity until the cell becomes unoccupied by reset. To plan a collision-free motion from a start configuration to a goal configuration, we first check collision of a direct path as it has the absolute shortest distance. Collision checking requires voxelization of the swept volume described in Section 2.2.3. During the process, collision is detected if any cell is found occupied. If direct path fails, we connect the two configurations to the roadmap via  $K$ -nearest neighbor search and collision checking. Not all  $K$  neighbors are necessarily examined. We start checking from the nearest neighbor to the most distant neighbor and stop if a collision-free edge is found. To search the path, A\* graph search algorithm (Hart et al., 1968) is used due to its superior performance in pathfinding. If the length of path is not infinite, we considered a collision-free path found. The path consists of a sequence of configurations. Since they are randomly generated, the robotic manipulator may not undergo a smooth motion. To further reduce the travel distance, we remove unnecessary nodes in the path. If there are only two nodes and the path between them are collision-free, one of them can be deleted. Otherwise, starting from the first node, we examine the path between node  $n^i$  and node  $n^{i+2}$  for collision. If the path is collision-free, node  $n^{i+1}$  is deleted and then the process is repeated until 1) node  $n^{i+2}$  is or beyond the last node after a deletion or 2) collision is detected between node  $n^i$  and node  $n^j$ . If node  $n^j$  is not the last node, the trimming process restarts at node  $n^j$ .

### 2.3. 3D Mapping In a Growth Chamber

The 3D environment in a growth chamber can be quickly mapped with Kinect V2 installed on the end-effector. Several poses above the plants can be manually selected as long as all plants can be imaged in the bird's eye view. We chose to set the poses as high as possible to increase field of view and reduce number of images required. A typical issue with ToF sensor is flying pixels near surface boundary. They are unreliable depth measurements which also occupy 3D space. We filter each depth image by thresholding the maximum absolute difference of the depth value between the center pixel and every neighbor's in a  $5 \times 5$  window.

The depth image is then converted to a 3D point cloud and transformed back to the base coordinate system of robotic manipulator based on

$$\mathbf{p}_{base} = T_{base2hand} T_{hand2cam} \mathbf{p}_{cam} \quad (1)$$

where  $\mathbf{p}_{cam}$  and  $\mathbf{p}_{base}$  denote the  $4 \times 1$  homogeneous coordinates of a point in camera coordinate system and in robot base coordinate systems, respectively,  $T_{hand2cam}$  and  $T_{base2hand}$  the  $4 \times 4$  homogeneous transformation matrices from end-effector pose to camera pose and from robot base to end-effector pose, respectively.  $T_{base2hand}$  comes from the forward kinematics given a configuration and the Denavit-Hartenberg parameters of the robotic manipulator.  $T_{hand2cam}$  can be estimated via hand-eye calibration. Since hand-eye calibration is well developed for regular 2D camera, we adopted the classic 2D approach using the intensity image of the ToF sensor instead of the depth image.  $T_{hand2cam}$  is solved by the least-squares solution proposed by Park et al. (1994).

After the multi-view registration, the point cloud does not have a uniform point density. There would be more point in the overlapping regions. To reduce unnecessary computation for the rest of the processing pipeline, the point cloud is downsampled and regularized with VoxelGrid filter (Rusu, 2010).

### 2.4. Individual Plant Extraction and Scanning

Given the known geometry and dimensions of the grow chamber, the plants including the pots can be cropped out of the 3D point cloud of the growth chamber environment by thresholding the ranges of  $x$ ,  $y$  and  $z$  coordinates. The next step is to resolve location and size of each plant and determine the scanning trajectory of the 2D laser profilometer. Normally the number of plants/pots in a growth chamber is fixed from beginning of an experiment.  $K$ -means clustering is used to partition the points into clusters representing individual plants. An axis-aligned bounding box is extracted for each cluster and the top face defines our scanning region.

A 2D laser profilometer works as follows. It emits a thin laser sheet and detect the laser on object surface with a 2D camera. The depth of any pixel on the laser line is calculated via triangulation. Therefore, to scan a 3D plant, we use the robotic manipulator to create a translational motion for the 2D laser profilometer, resulting the laser line covering the top canopy.

The translation motion of the end-effector undergoes three phases, acceleration, constant speed and deceleration. And its speed profile over time is a trapezoid. Assuming that the 2D laser profilometer starts scanning and moving at the same moment with a constant scan frequency  $f$ , the time when line profile number  $n$  is being scanned is calculated as

$$t = \frac{n-1}{f}. \quad (2)$$

Then the  $3 \times 1$  translation vector  $\mathbf{v}_n$  for scan number  $n$  with respect to the scan starting pose is calculated as

$$\mathbf{v}_n = \begin{cases} \frac{1}{2}at^2\hat{\mathbf{v}}, & t < t_a \\ V\left(t - \frac{t_a}{2}\right)\hat{\mathbf{v}}, & t_a \leq t \leq t_d \\ \left\{V(t - t_d) - \frac{d(t-t_d)^2}{2}\right\}\hat{\mathbf{v}}, & t_d < t \end{cases} \quad (3)$$

where  $a$  denotes acceleration constant,  $d$  deceleration constant,  $t_a$  the time when acceleration ends,  $t_d$  the time when deceleration starts,  $V$  velocity constant,  $\hat{\mathbf{v}}$  the  $3 \times 1$  normalized translation vector for the end-effector. A point  $\mathbf{q}_{scan}^n$  in scan  $n$  is transformed to the point  $\mathbf{p}_{base}^n$  in the robot base frame based on

$$\mathbf{p}_{base}^n = T_{base2hand}T_{hand2scan} \left( \mathbf{q}_{scan}^n + \mathbf{v}_n \right) \quad (4)$$

where  $T_{hand2scan}$  denotes the transformation matrix from end-effector to 2D laser profilometer.  $T_{hand2scan}$  is determined via hand-eye calibration. Note that  $\mathbf{q}_{scan}^n$  is not in homogeneous coordinates. We used the method proposed by Carlson et al. (2015) for hand-eye calibration between a 2D laser profilometer and a 6-DOF robotic manipulator using planar constraints. One only needs to collect multiple line scans on a plane and repeat the process for multiple planes. The optimization procedure starts with an initial guess and iteratively optimizes first the rotation matrix and then the translation vector to minimize the sum of squared distance from the points to the associated planes. The advantage is that it mainly involves well-developed methods, Principle Component Analysis (PCA), Ordinary Least Squares and Singular Value Decomposition.

## 2.5. Leaf Segmentation and Extraction of Probing Locations and Directions

The high-precision 3D scan using the 2D laser profilometer enables accurate surface normal estimation. Surface normal is estimated based on PCA of local neighborhood around a 3D point. More specifically, eigenvalue decomposition is performed on the  $3 \times 3$  covariance matrix for the set of points. Surface normal is then approximated by the normalized eigenvector corresponding to the minor eigenvalue.

As plant leaf surface tends to be smooth, neighboring points on the same leaf should have similar surface normal direction and low curvature. We applied the region growing segmentation with smoothness constraint (Rabbani et al., 2006) for leaf segmentation. An implementation is available in Point Cloud Library (PCL, Rusu and Cousins, 2011). It starts with a seed defined by the point of minimum curvature and then merges a neighbor if 1) the angle between the seed's normal and the neighbor's normal is less than a threshold and 2) the plane fitting residual with  $K$ -nearest neighbors is less than a threshold. If a neighbor is merged, it is queued as a new seed. Once all the neighbors of a seed are evaluated, the seed is removed from the queue. The region growing stops when there is no seed left in the queue. The visited points are labeled. Then the same process is repeated on the rest unlabeled points until all points are labeled.

The segmentation results can be further filtered based on size and position. Each segment is a piece-wise smooth point cluster. Moreover, the scanned point cloud is downsampled with VoxelGrid filter and each voxel in 3D space contains at most 1 point. Therefore, segment surface area can be estimated by the product of the number of points in the cluster and the voxel size. Segment position is represented by the cluster centroid.

Many locations on a leaf segment may be probed free of collision, especially for elongate leaf shape. Voxel Cloud Connectivity Segmentation (Papon et al., 2013) is used to efficiently partition a leaf segment into several small patches of similar sizes, namely, supervoxels. The potential probing locations are based on the supervoxels with low RMS values of plane fitting. Although leaf surface is smooth, it is desirable to probe a planar patch which leads to an accurate surface normal estimate. Supervoxel size is a user-defined parameter to control the surface patch size and is reasonable to set to a value based on the diameter of the probe. Finally, the probing location is chosen to be the point closest to the centroid of the supervoxel and the probing direction is parallel to the normal of the plane fitted to the supervoxel.

## 2.6. Probing Pose Determination

A probing stick is mounted next to the laser profilometer parallel to the  $z$ -axis of robot tool frame (the last reference frame in Figure 2). The probe tip position in robot tool frame was obtained by tool center point (TCP) calibration. A number of robot tool frames were recorded as the robot end-effector was moved such that the probe tip stayed at a fixed point in 3D space while the probe body were rotated around that point. Every pair of frame  $i$  and frame  $j$  forms a linear equation,

$$(R_j - R_i) \begin{bmatrix} X_p \\ Y_p \\ Z_p \end{bmatrix} = T_i - T_j \quad (5)$$

where  $R$  and  $T$  denote the rotation matrix and the translation vector of robot tool frame, respectively. The probe tip position  $[X_p, Y_p, Z_p]^T$  can be solved in a least-squares fashion. Figure 4 illustrates one of several robot tool frames recorded for TCP calibration. Given a probing pose  $T_{base2probe}$ , the robot tool frame is simply calculated as

$$T_{base2tool} = T_{base2probe} \begin{bmatrix} 1 & 0 & 0 & -X_p \\ 0 & 1 & 0 & -Y_p \\ 0 & 0 & 1 & -Z_p \\ 0 & 0 & 0 & 1 \end{bmatrix}. \quad (6)$$

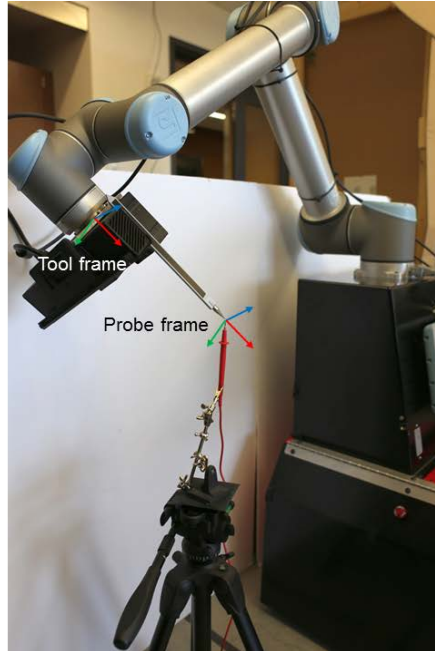


**Figure 4. Probe tip calibration.** The end-effector was carefully guided with teach pendant to a pose where the probe tip touched the calibration probe tip. Tool frame refers to the last reference frame of robotic manipulator. Probe frame is obtained by translating tool frame to probe tip. Red arrow: X-axis; Green arrow: Y-axis; Blue arrow: Z-axis.

Without loss of generality, we address probing a point on plant leaf surface with the probe perpendicular to the local surface patch. Given a probing point and its normal direction, the probing pose is not uniquely defined. The robot tool frame may rotate around the surface normal axis provided that the robot does not self-collide (Section 2.2.1.) or collide with the environment (Section 2.2.3.; Section 2.2.4.). The solution set could be infinite but only one solution is required. Therefore, we test a finite number of probing pose candidates which are end-effector poses rotated around the surface normal axis with a step size of 10 degrees. Among the collision-free candidates, we select the one with least rotation of the last wrist joint. Note that this choice is arbitrary. To compute the robot configuration given a tool frame, we use the analytic inverse kinematics solutions implemented in the ROS (Quigley et al., 2009) package *ur\_kinematics* (Hawkins, 2013).

### 3. Experiments and Results

Except calibration, all the experiments were conducted with a growth chamber mock-up in front of the robot and 4 pots of artificial plants placed in a row at the center of the chamber floor. The pot size was 0.28 m in diameter and the plant height was approximately 0.28 m. The average leaf length and maximum leaf width were 0.13 m and 0.03 m, respectively. The sensors and the robotic manipulator were controlled by an industrial PC equipped with an Intel Core i5-4300U CPU clocked at 1.9 GHz with 8 GB RAM. We utilized OpenCV and PCL for 3D perception and visualization. PRMCE was implemented using the Boost Graph Library for building the roadmap and A\* graph search. The precomputed data structure was saved and loaded with Boost Serialization Library. *K*-nearest neighbor search was done by using the FLANN library (Muja and Lowe, 2009). Figure 5 illustrates the workflow of the robotic leaf probing pipeline. The purposes of the following experiments were to evaluate the key aspects of the pipeline.

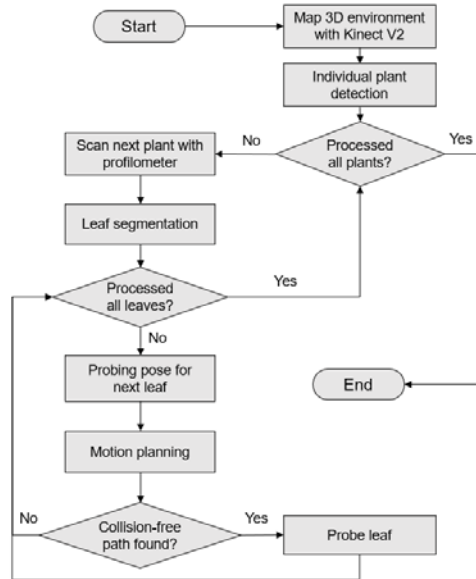


Figure 5. Workflow of the robotic leaf probing pipeline.

### 3.1. Calibration

For TCP calibration, 8 random robot tool frames were recorded for probing a calibration probe tip fixed in robot base frame. For each data acquisition, the teach pendant was used to carefully orient and position the probe (Figure 4). 56 pairs of poses formed equal number of linear equations. The least-squares solution resulted in a translation vector of the probe tip in robot tool frame  $(0.0866, 0.0268, 0.2485)^T$ . Since the position of the calibration probe tip was unknown in robot base frame, we compute the probe tip positions in robot base frame with the TCP calibration result and present the standard errors of the means of probe tip positions in X, Y and Z dimensions (Table 1). The errors also include human error when aligning the robot probe tip and calibration probe tip.

Table 1. Standard errors of the means of 8 probe tip positions in robot base frame in X, Y and Z dimensions.

Dimension	X	Y	Z
Standard Error (mm)	0.1686	0.1629	0.1772

For hand-eye calibration of the laser profilometer, 9 planes with different orientations were used and 6 lines on each plane were scanned to estimate the plane equation. In total, 32681 data points were acquired. Figure 6 shows scanning a line on one plane with the laser profilometer.

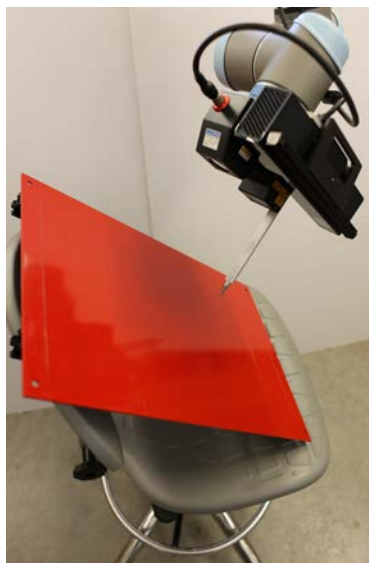


Figure 6. Scanning a line on a plane for laser profilometer hand-eye calibration.

Our initial hand-to-eye transformation was started with

$$T_{hand2scanner} = \begin{bmatrix} 0 & 1 & 0 & 0.076 \\ -1 & 0 & 0 & 0 \\ 0 & 0 & 1 & 0.094 \\ 0 & 0 & 0 & 1 \end{bmatrix}.$$

The optimization was run for 10 iterations, returning the final estimate

$$T_{hand2scanner} = \begin{bmatrix} 0.0066 & 0.9999 & -0.0087 & 0.0761 \\ -0.9999 & 0.0067 & 0.0042 & 0.0018 \\ 0.0043 & 0.0087 & 0.9999 & 0.0941 \\ 0 & 0 & 0 & 1 \end{bmatrix}.$$

The root mean squared (RMS) distance between the points to their associated planes is illustrated in Figure 7. The final RMS distance was 0.3951 mm.

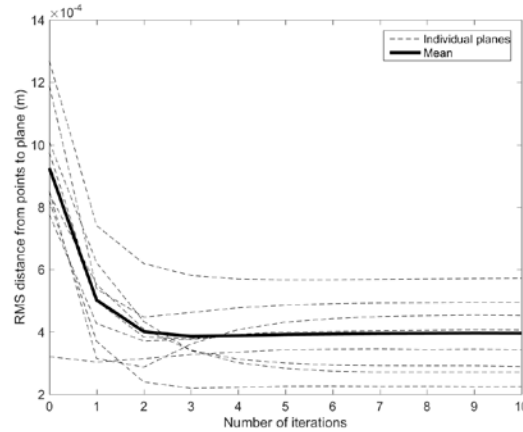


Figure 7. Convergence results for profilometer hand-eye calibration data gathered from 9 planes. The RMS distance between measurement points and their associated planes are shown for individual planes and the mean over all planes.

### 3.2. 3D Mapping and Plant Perception

The environment inside the growth chamber mock-up was mapped with 3 views. The 3D point cloud of the environment was regularized by VoxelGrid filter to the resolution of 2 mm whenever a new view was merged. Part of the growth chamber mock-up was built into the robot model. The mapping aimed to capture the plants and the side walls which were not modeled as the robot in case that the robot needed to crab to a side location and relocalize itself relative to the center location by mapping the side walls. In this study, for the evaluation of collision-free leaf probing, it was sufficient to test the center location. After cropping out the plants, individual plants were segmented by using the implementation of *K*-means clustering in OpenCV which supports a robust seeding procedure (Arthur et al., 2007). Figure 8 illustrates the mapping and plant segmentation process.

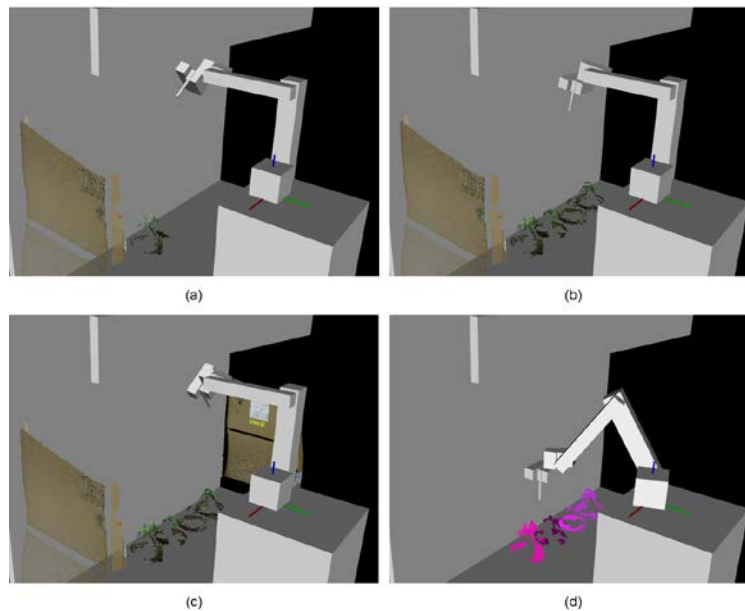


Figure 8. 3D mapping in the growth chamber mock-up and plant segmentation. (a) Imaging pose 1. (b) Imaging pose 2. (c) Imaging pose 3. (d) Plant segmentation via K-means clustering.

Each plant was scanned with the laser profilometer at a sweeping speed of 0.1 m/s with a scanning rate of 2000 Hz. The scan line width of the laser profilometer was 0.11 m at the minimum working distance (0.155 m) and 0.24 m at the maximum working distance (0.445 m). The point cloud was then filtered through a voxel grid of size 1 mm. Large leaf segments were found by region growing segmentation and planar small patches were extracted by supervoxel segmentation. The key parameters of the two segmentation algorithms are listed in Table 2 and Table 3. Figure 9 demonstrates the extracted leaf segments and potential probing locations. A supervoxel segment was considered as a probing candidate if the RMS value of plane fitting was less than 0.5 mm.

**Table 2. Key parameters for region growing segmentation.**

Number of neighbors	Residual threshold	Smoothness threshold	Minimum cluster size	Maximum cluster size
6	0.01	7 deg	1000	10000

**Table 3. Key parameters for supervoxel segmentation.**

Voxel resolution	Seed resolution	Spatial importance	Normal importance
0.001 m	0.02 m	0.5	1.0

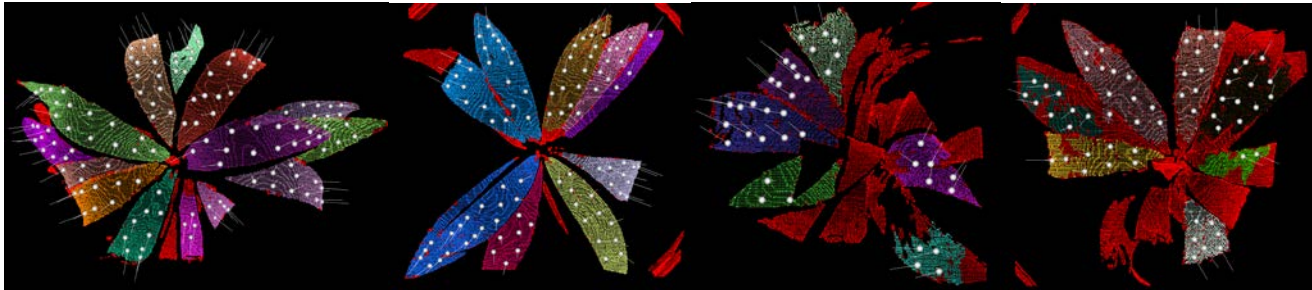


**Figure 9 . Leaf segmentation results and probing location candidates. The images are top views of the 3D point clouds scanned by the laser profilometer. Red points are rejected by region growing segmentation. Any other color represents a different leaf segment. A probing location candidate is shown with a sphere and the surface normal direction.**

### 3.3. Robotic Probing Accuracy

To quantify probing error in terms of position and orientation, we used the full system to scan and probe the centroid of a  $0.09 \times 0.09$  m square surface of a calibration block with different orientations. The calibration block was first placed in front of the robot such that the square edges were either parallel or perpendicular to the X-axis and the Y-axis of robot base frame. As a result, the square surface was perpendicular to the Z-axis of robot base frame. Then the square surface was scanned such that the laser sheet was perpendicular to the surface and parallel to the Y-axis moving in X direction. Figure 10 illustrates our scanning setup.

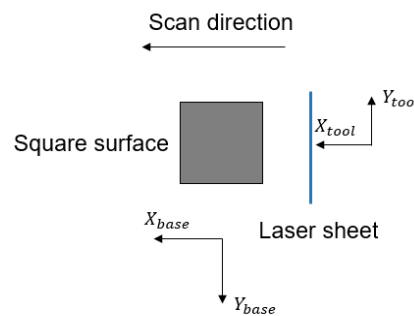


**Figure 10. Top view of the scanning setup for robotic probing accuracy test.**

The rest of our processing pipeline would automatically extract the square surface as well as the probing pose and execute probing. Once the probe reached its destination, the position of robot tool frame was recorded as  $t_{robot}$ . Figure 11 shows probing the square centroid perpendicularly. Then probe was carefully guided in absolute translation by using teach pendant to probe the physical centroid, resulting a new position of robot tool frame,  $t_{manual}$ . Probing position error is defined as the Euclidean distance between  $t_{robot}$  and  $t_{manual}$ . As for probing orientation, the angle between the probe and the square surface was measured and the error was defined as the absolute deviation from 90 degrees due to perpendicular probing. The angle was measured by using a digital protractor with an accuracy of  $\pm 0.1$  degrees. The full process was repeated three times. In addition to the leveled surface, the same process was done when the calibration block was rotated around X-axis and Y-axis of the robot base frame, respectively, by  $0$ ,  $\pm 30$ , and  $\pm 60$  degrees. The results of probing position errors and angle errors with different surface orientations are shown in Figure 12. In summary, our system achieved a probing position error of  $1.5 \pm 0.20$  mm and a probing angle error of  $0.84 \pm 0.18$  degrees with a 95% confidence interval. In addition, 5 examples of the probing poses executed by our system is illustrated in Figure 13.



Figure 11. Probing the centroid of  $0.09 \times 0.09$  m square surface perpendicularly.

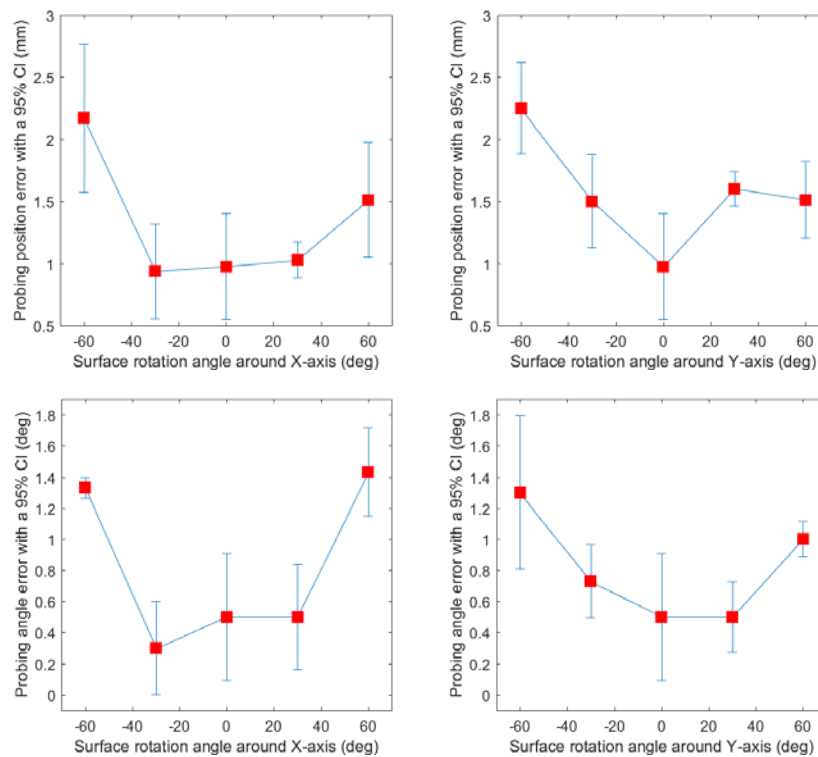


Figure 12. Probing errors with different surface orientations. Each surface orientation was probed three times. Top left: probing position error when the square surface was rotated around X-axis of robot base frame. Top right: probing position error when the square surface was rotated around Y-axis of robot base frame. Bottom left: probing angle error when the square surface was rotated around X-axis. Bottom right: probing angle error when the square surface was rotated around Y-axis.



Figure 13. Leaf probing pose examples performed by our system.

### 3.4. Motion Planning

The PRMCE motion planner was evaluated in terms of planning time and path quality. The full robotic leaf probing routine was tested on this experimental setting. The plants were processed in a decreasing order of their X coordinates in robot base frame. For each plant, the leaf segments were probed in the same order. For each leaf segment, the maximum number of probing locations allowed was set to 1.

The key parameters for the planner are number of nodes, number of neighbors per node, and 3D occupancy grid size. They were set to 5000, 20, and 0.04 m, respectively. As a result, generating the reusable roadmap took 37 minutes and the precomputed data structure occupied ~1 GB RAM, but loading the file only took ~2.5 s.

In total, 16 leaf segments were found that the collision-free probing pose existed. And all of them were successfully probed without collision. Motion planning happened when the robotic manipulator needed to move from one probing pose to the next. The planning was broken down into three stages: *Stage 1*. connecting to roadmap; *Stage 2*. A\* graph search; *Stage 3*. path smoothing. Table 4 illustrates the average time and standard deviation for each stage. The average planning time and standard deviation were 416.3 ms and 355.6 ms.

**Table 4. Average time and standard deviation of the three stages of motion planning.**

Stage	Average time (ms)	Standard deviation (ms)
Connecting to roadmap	138.6	52.3
A* graph search	1.2	0.4
Path smoothing	276.5	320.2

The traveled distances of two reference points on the robotic manipulator were used to quantify path quality, one at the tool frame (*Frame 6* in Figure 2) and one at the elbow frame (*Frame 2* in Figure 2). The elbow point was included for it connects the two longest arms of UR 10. Table 5 shows the average traveled distance and standard deviation for each reference point. Figure 14 illustrates some collision-free paths found by PRMCE in our experiment.

**Table 5. Traveled distances of tool frame and elbow frame of UR 10.**

Reference point	Average traveled distance (m)	Standard deviation (m)
Tool	1.06	0.20
Elbow	0.92	0.18

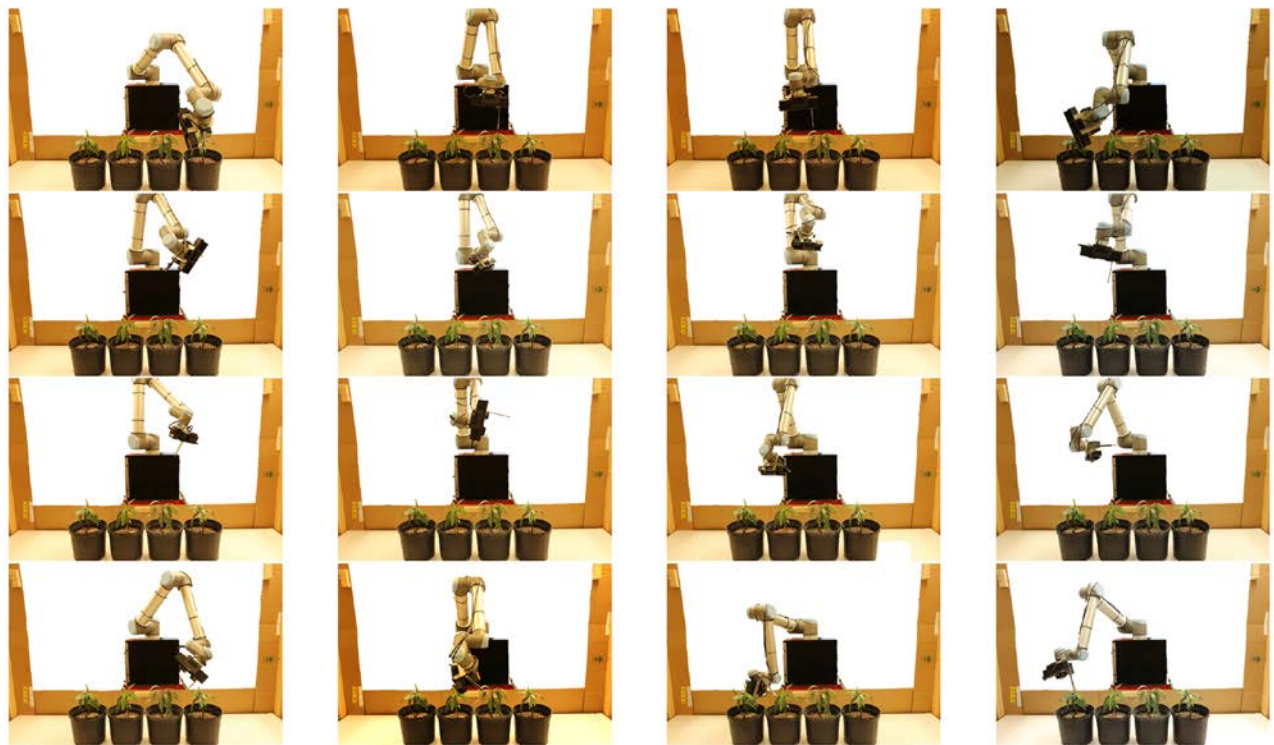


**Figure 14. Collision-free path examples found by PRMCE. Each column represents one path where the first image shows the starting pose and the last the goal pose. The background is removed for better visualization.**

## 4. Discussion

First of all, the achieved average probing accuracy was highly promising for automated instrumentation with probes. It would not be possible without accurate TCP and hand-eye calibrations. Meanwhile, the robotic probing results suggested that the errors of both probing position and probing angle tended to increase as the object surface became more slanted with respect to the laser profilometer. One possible reason for such behavior is the decrease in spatial resolution of the point cloud data when the slanted surface was scanned. For leaf probing application, the problem can be solved by rescanning each leaf segment in a frontal-parallel way although it would require more operation time. Another source of error was the uncertain delay between the time when the robotic manipulator started moving and the time when the laser profilometer started scanning. The UR10 was remotely controlled via TCP/IP and the laser profilometer was triggered using its software development toolkit. It is possible to improve the probing accuracy if the robotic manipulator and the laser profilometer are synchronized via hardware.

With high-precision laser scan, region growing segmentation with smoothness constraint was able to extract large piecewise smooth leaf surfaces. On the other hand, overlapping leaves with similar surface normal directions tended to be merged as one segment. Using RMS value of plane fitting on the supervoxel as a criterion to filter potential probing locations worked as expected, especially when a supervoxel belonged to the edges of two overlapping leaves.

The motion planning experiment showed that the PRMCE planner was both fast and effective for robotic leaf probing in a growth chamber environment. As for planning time, *Stage 1* took approximately one third of the total time. In this stage, the planner searched for the nearest configurations on the roadmap that could connect to the start and the goal configurations without collision. In addition to  $K$ -nearest neighbor search, it required collision checking up to  $K$  times for the start and the goal configurations, respectively. In *Stage 2*, the planner searched for a path on the roadmap. A\* graph search proved to be highly efficient. The average time took  $\sim 1$  ms, which was neglectable compared to the other two stages. In *Stage 3*, unnecessary waypoints were removed in the path found in *Stage 2*. The running time depended on the number of waypoints in the original path and the specific scenario of the 3D workspace occupancy, hence resulting in a large standard deviation. Collision checking remained a major bottleneck since it required 3D voxelization of the OBBs representing the robotic manipulator and sensors. Its computational complexity largely depends on the size of 3D occupancy grid. The smaller the grid size is, the more 3D cells are visited, and the more accurate the collision checking is. Note that collision checking can be done independently for each OBB. Further speedup can be achieved by parallel 3D voxelization of the OBBs with modern multi-core CPUs. Regarding path quality, the paths found by PRMCE for moving from one probing pose to another were reasonable. Usually the path included two intermediate waypoints as shown in Figure 14. The first waypoint moved the end-effector safely away from the start configuration to a position higher than the plants. The second one served a similar purpose for the goal configuration. Since our probe was fairly long (0.26 m), a path with only one intermediate waypoint was less likely to be collision-free.

## 5. Conclusion

An eye-in-hand robotic system was developed to perform automated high-throughput 3D plant perception and leaf probing with real-time collision-free motion planning for a growth chamber environment. Rapid environment mapping was realized by several shots with Kinect V2 depth sensor guided by a 6-axis robotic manipulator. The resulting 3D point cloud served for both the workspace occupancy status around the robot and individual plant detection via K-means clustering. PRMCE allowed for real-time motion planning that avoided collision between the robot and the environment. High-precision 3D scanning of plant canopy was obtained by sweeping a 2D laser profilometer with the robotic manipulator at a close distance. 3D region growing segmentation was used to find large leaf segments. They were further partitioned into supervoxels upon which probing locations and probing angles were computed. The adopted TCP and hand-eye calibration required simple procedures to acquire data and the results were accurate. For probing the centroid of a square surface, the average system errors of probing position and probing angle were 1.5 mm and 0.84 degrees, respectively. The PRMCE motion planner was tested using the proposed robotic leaf probing pipeline in a scenario where 4 pots of artificial plants were placed in a growth chamber mock-up. All 16 leaves found feasible to be probed were successfully probed without collision. The average motion planning time was 416.3 ms and the average traveled distances of tool frame and elbow frame were approximately 1 m. For future work, we plan to equip the robot with a fluorimeter and a Raman spectrometer and evaluate how the probing accuracy affects the instrumentation on real plants. How to adapt the system for different plant types and growth stages also remains a valuable research topic.

### Acknowledgements

This work is supported by National Science Foundation under the project “MRI: Development of an ENVIRATRON – an accelerator for climate change research”.

## References

- Ahlin, K., Joffe, B., Hu, A. P., McMurray, G., & Sadegh, N. (2016). Autonomous Leaf Picking Using Deep Learning and Visual-Servoing. *IFAC-PapersOnLine*, 49(16), 177-183.
- Alenya, G., Dellen, B., Foix, S., & Torras, C. (2013). Robotized plant probing: Leaf segmentation utilizing time-of-flight data. *IEEE Robotics & Automation Magazine*, 20(3), 50-59.
- Arthur, D., & Vassilvitskii, S. (2007, January). k-means++: The advantages of careful seeding. In *Proceedings of the eighteenth annual ACM-SIAM symposium on Discrete algorithms* (pp. 1027-1035). Society for Industrial and Applied Mathematics.
- Carlson, F. B., Johansson, R., & Robertsson, A. (2015, September). Six DOF eye-to-hand calibration from 2D measurements using planar constraints. In *Intelligent Robots and Systems (IROS), 2015 IEEE/RSJ International Conference on* (pp. 3628-3632). IEEE.
- Cohen-Or, D., & Kaufman, A. (1997). 3D line voxelization and connectivity control. *IEEE Computer Graphics and Applications*, 17(6), 80-87.
- Eberly, D. (2002). Dynamic collision detection using oriented bounding boxes. *Geometric Tools, Inc.*
- Foix, S., Alenya, G., & Torras, C. (2015, September). 3D Sensor planning framework for leaf probing. In *Intelligent Robots and Systems (IROS), 2015 IEEE/RSJ International Conference on* (pp. 6501-6506). IEEE.
- Hart, P. E., Nilsson, N. J., & Raphael, B. (1968). A formal basis for the heuristic determination of minimum cost paths. *IEEE transactions on Systems Science and Cybernetics*, 4(2), 100-107.
- Hawkins, K. P. (2013). *Analytic inverse kinematics for the universal robots UR-5/UR-10 arms*. Georgia Institute of Technology.
- Kavraki, L. E., Svestka, P., Latombe, J. C., & Overmars, M. H. (1996). Probabilistic roadmaps for path planning in high-dimensional configuration spaces. *IEEE transactions on Robotics and Automation*, 12(4), 566-580.
- Kunz, T., Reiser, U., Stilman, M., & Verl, A. (2010, October). Real-time path planning for a robot arm in changing environments. In *Intelligent Robots and Systems (IROS), 2010 IEEE/RSJ International Conference on* (pp. 5906-5911). IEEE.
- Lachat, E., Macher, H., Mittet, M. A., Landes, T., & Grussenmeyer, P. (2015). First experiences with Kinect v2 sensor for close range 3D modelling. *The International Archives of Photogrammetry, Remote Sensing and Spatial Information Sciences*, 40(5), 93.
- LaValle, S. M. (1998). Rapidly-exploring random trees: A new tool for path planning.
- Leven, P., & Hutchinson, S. (2002). A framework for real-time path planning in changing environments. *The International Journal of Robotics Research*, 21(12), 999-1030.
- Muja, M., & Lowe, D. G. (2009). Fast approximate nearest neighbors with automatic algorithm configuration. *VISAPP (1)*, 2(331-340), 2.
- Murray, S., Floyd-Jones, W., Qi, Y., Sorin, D., & Konidaris, G. (2016, June). Robot motion planning on a chip. In *Robotics: Science and Systems*.
- Newcombe, R. A., Izadi, S., Hilliges, O., Molyneaux, D., Kim, D., Davison, A. J., ... & Fitzgibbon, A. (2011, October). KinectFusion: Real-time dense surface mapping and tracking. In *Mixed and augmented reality (ISMAR), 2011 10th IEEE international symposium on* (pp. 127-136). IEEE.
- Papon, J., Abramov, A., Schoeler, M., & Worgotter, F. (2013). Voxel cloud connectivity segmentation-supervoxels for point clouds. In *Proceedings of the IEEE Conference on Computer Vision and Pattern Recognition* (pp. 2027-2034).
- Park, F. C., & Martin, B. J. (1994). Robot sensor calibration: solving  $AX=XB$  on the Euclidean group. *IEEE Transactions on Robotics and Automation*, 10(5), 717-721.
- Quigley, M., Conley, K., Gerkey, B., Faust, J., Foote, T., Leibs, J., ... & Ng, A. Y. (2009, May). ROS: an open-source Robot Operating System. In *ICRA workshop on open source software* (Vol. 3, No. 3.2, p. 5).
- Rabbani, T., Van Den Heuvel, F., & Vosselmann, G. (2006). Segmentation of point clouds using smoothness constraint. *International archives of photogrammetry, remote sensing and spatial information sciences*, 36(5), 248-253.
- Rusu, R. B. (2010). Semantic 3d object maps for everyday manipulation in human living environments. *KI-Künstliche Intelligenz*, 24(4), 345-348.
- Rusu, R. B., & Cousins, S. (2011, May). 3d is here: Point cloud library (pcl). In *Robotics and Automation (ICRA), 2011 IEEE International Conference on* (pp. 1-4). IEEE.
- Schulz, H., & Baranska, M. (2007). Identification and quantification of valuable plant substances by IR and Raman spectroscopy. *Vibrational Spectroscopy*, 43(1), 13-25.
- Shah, D., & Tang, L. (2016, July). Development of an Autonomous Indoor Phenotyping Robot. In *2016 ASABE Annual International Meeting* (p. 1). American Society of Agricultural and Biological Engineers.
- Shah, D., Tang, L., Gai, J., & Putta-Venkata, R. (2016). Development of a Mobile Robotic Phenotyping System for Growth Chamber-based Studies of Genotype x Environment Interactions. *IFAC-PapersOnLine*, 49(16), 248-253.